NASA TN D-853

C4 (3)
FTT
FILES
S&T
2264-2-3-4

NASA TN D-853

TECHNICAL NOTE

D-853

AN INVESTIGATION OF TRANSONIC FLOW FIELDS SURROUNDING

HOT AND COLD SONIC JETS

By George Lee

Ames Research Center
Moffett Field, Calif.

NATIONAL AERONAUTICS AND SPACE ADMINISTRATION

WASHINGTON April 1961

1E

NATIONAL AERONAUTICS AND SPACE ADMINISTRATION

TECHNICAL NOTE D-853

AN INVESTIGATION OF TRANSONIC FLOW FIELDS SURROUNDING HOT AND COLD SONIC JETS

By George Lee

SUMMARY

An investigation at free-stream Mach numbers of 0.90 to 1.10 was made to determine (1) the jet boundaries and the flow fields around hot and cold jets, and (2) whether a cold-gas jet could adequately simulate the boundary and flow field of hot-gas jet. Schlieren photographs and static-pressure surveys were taken in the vicinity of a sonic jet which was operated over a range of jet pressure ratios of 1 to 6, specific heat ratios at the nozzle exit of 1.29 and 1.40, and jet temperatures up to 2600° R.

It was found that the jets induced shock waves in the flow fields at sonic and supersonic stream velocities. Results indicated that the jet boundaries, shock waves, and pressure distributions in the flow field around a hot jet could be duplicated satisfactorily by a cold jet when the specific heat ratio and jet pressure ratio were matched.

INTRODUCTION

A problem that has proven to be of some concern in the design of turbojet and rocket-propelled aircraft and missiles is the effect of jet exhaust on the flow over adjacent components of the vehicle. The aerodynamic effects induced by a jet can appear as changes in stability, trim and drag. The changes can be either favorable or unfavorable, depending upon the vehicle geometry, flight conditions, and jet-exhaust characteristics. An example of unfavorable changes is provided by reference 1 which showed that the longitudinal trim of a free-flight model was greatly altered by a jet. Reference 2 provides an example of favorable changes; it was shown therein that sizable reductions in drag can be achieved by use of jet-exhaust interference on an afterbody. Because of the possible importance of the jet-interference effects, there has, of course, been a demand by designers for information which will allow them to properly cope with the jet-interference effects. The need for information became particularly acute as the flight speeds of aircraft and missiles extended into the transonic and supersonic ranges where jet exhausts can introduce strong shock waves into the external flow.

The research on jet-interference effects can be divided into the following three phases: (1) determination of the jet-flow characteristics (i.e., internal flow and jet boundary), (2) determination of the external flow disturbances associated with the particular jet-flow characteristics, and (3) determination of the aerodynamic reaction of vehicle surfaces immersed in the disturbed flow. Progress in this research has been greater for supersonic speeds than for transonic speeds. Primarily, this was due to the fact that theoretical methods, such as linearized potential theory and the method of characteristics, were applicable for the supersonic case but were not so readily applicable for the transonic case. This has led to an understanding of the problem at supersonic speeds (refs. 3 to 13) and has resulted in an analytical procedure for using a cold-air jet to simulate the interference effects of hot jets at supersonic speeds (refs. 3 and 9). However, experimental data confirming this procedure is still rather scant. The research at transonic speeds, on the other hand, has essentially been confined to the determination of the gross changes in the aerodynamic characteristics of complete airplanes and missiles due to jet effects. This course of research has been dictated largely by (1) an urgent need for the jet-effect information and (2) the difficulty of the analytical approach. For these reasons, various experimenters have used simple cold-air jets which may not adequately simulate the hot-jet effects, or they have used a complex, hazardous, and costly technique, such as the hydrogen-peroxide jet described in reference 14. Clearly then, there is room for increasing the knowledge at transonic speeds of jet-exhaust characteristics and their effects on the external flow.

A particularly useful direction to take in further research on jet effects at transonic speeds is a study of the possibility of using cold-gas jets to simulate the effects of hot jets on the external flow. This report presents the results of an exploratory investigation of this possibility for a particular nozzle and afterbody geometry. In the investigation, a model with a sonic nozzle was operated with hot and cold gases over ranges of jet to free-stream static-pressure ratios of 1 to 6, free-stream Mach numbers from 0.9 to 1.10, jet specific heat ratios of 1.29 and 1.40, and jet stagnation temperatures of 520° R to approximately 2600° R. Combustion of hydrogen and air provided the hot jet. Air or carbon dioxide was used for the cold jets. Stagnation temperatures and schlieren photographs were obtained in studying the internal jet flow characteristics. Static-pressure surveys and schlieren photographs of the external flow field were made to determine the effects of the jet on the external flow field.

SYMBOLS

B_j $\sqrt{M_j^2 - 1}$

c reference length equal to instrumented length of cone-cylinder pressure tube (6-3/4 nozzle diameters)

ΔC_N	incremental normal-force coefficient, $\dfrac{N_{on} - N_{off}}{q_\infty S}$
ΔC_m	incremental pitching-moment coefficient, $\dfrac{L_{on} - L_{off}}{q_\infty Sc}$
C_p	pressure coefficient, $\dfrac{p - p_\infty}{q_\infty}$
ΔC_p	incremental pressure coefficient, $C_{p_{on}} - C_{p_{off}}$
d	diameter of jet
d_j	diameter of nozzle
d_w	diameter of jet at the end of the primary wavelength
L	moment, $\int_{x/d_j=-0.75}^{x/d_j=6} C_p \frac{x}{d_j} d\left(\frac{x}{d_j}\right)$
M_∞	free-stream Mach number
M_j	jet Mach number
N	normal force, $\int_{x/d_j=-0.75}^{x/d_j=6} C_p d\left(\frac{x}{d_j}\right)$
p_j	static pressure at the nozzle exit
p_∞	free-stream static pressure
q_∞	free-stream dynamic pressure, $\frac{1}{2}\rho_\infty V_\infty^2$
R	$R = \frac{1}{2}(d - d_j)$
S	reference area c (unit width)
V_∞	free-stream velocity
w	primary wavelength
x	axial distance downstream of nozzle exit
y	radial distance from jet axis

α inclination of jet shock with the free stream

β inclination of exit shock with the free stream

γ_j specific heat ratio at jet exit

δ initial slope of jet boundary

ρ_∞ free-stream density

φ velocity potential

Subscripts

on jet on

off jet off

WIND TUNNEL

The tests were made in the Ames 1- by 3-1/2-Foot Wind Tunnel which is a closed-circuit, atmosphere-density type tunnel. It employs perforated top and bottom walls for continuous operation at transonic speed. A detailed description of the wind tunnel is given in reference 15.

MODEL AND APPARATUS

A sketch of the model with principal dimensions is shown in figure 1. The model consisted of a nose cone, a hollow cylindrical midsection, and a convergent nozzle. A boundary-layer trip, which consisted of a 1/32-inch ring, was located near the midsection of the model. Within the midsection were the hydrogen burner and an orifice for measuring the pressure in the chamber surrounding the burner. The entire assembly was mounted to the side of the wind tunnel by a hollow strut which also served to conduct the hydrogen, air, and the carbon dioxide.

A 10-orifice cone-cylinder tube was used for pressure surveys. Dimensions of this tube are given in figure 2. A photograph of the survey tube and the model mounted in the wind tunnel is presented in figure 3. Thermocouples and an optical pyrometer were used to measure the gas temperatures at the nozzle.

TESTS

Sonic hot and cold jets were tested at free-stream Mach numbers of 0.9 to 1.10 and a Reynolds number of 4.68×10^6 based on model length. The jet static-pressure ratio was varied from 1 to 6. The hot-jet stagnation temperature was maintained at approximately 2600° R. At this temperature the specific heat ratio was estimated to be 1.29. The cold-air jet stagnation temperature was kept at room temperature. The carbon-dioxide jet was heated to approximately 580° R stagnation temperature so that its specific heat ratio matched that of the hot jet at the model exit station. Although carbon dioxide is an imperfect gas, it was used in this investigation because for the pressure ratios of these tests, its specific heat ratio variation and range are similar to those of the hot gas. Pressure surveys of the flow surrounding the jet were taken at the three radial positions shown in figure 4.

DATA REDUCTION

The static pressures measured on the cone-cylinder tube were reduced to the usual pressure coefficient form $C_p = (p - p_\infty)/q_\infty$. Static-pressure distributions in the external flow field around the jets were integrated to obtain normal force and moment coefficients. For convenience of integration, the reference length of the coefficients was arbitrarily chosen as the instrumented length of the cone-cylinder tube. A static-pressure ratio was determined between the jet static pressure at the nozzle exit and the free-stream static pressure. In this procedure the jet static pressure was calculated from the pressure taken in the model chamber and the free-stream static pressure was measured with an orifice located in the side of the test section. The linear and angular data from the schlieren photographs were read on an optical comparator. The linear data consisted of certain jet boundary dimensions, and the angular measurements consisted of the initial slopes of the jet boundary and the slopes of shock waves in the flow field surrounding the jet.

PRECISION

The precision of the schlieren data was primarily limited by the small size of the schlieren photographs. The small photographs resulted in jet images within the jet primary wavelength of approximately 1/8 by 1/4 inch. A secondary source of error was the poor definition in the photographs. This was especially the case for the hot-jet photographs. With these factors involved, the probable errors in the schlieren data are considered to be as follows:

Angular measurements ±1.5°

Linear measurements ±1 percent

The probable errors in the pressure and Mach number data, as determined by a root mean square analysis, are considered to be as follows:

C_p	±0.002
p_j/p_∞	±0.05
M_∞	±0.005

A
3
6
8

RESULTS AND DISCUSSION

Before presenting and discussing the quantitative evaluation of the simulation of the hot-jet interference by use of a cold jet, it is desirable to examine briefly the qualitative aspects of jet interference at transonic speeds. This qualitative examination will cover the different types of jet-interference patterns occurring in the transonic speed range. In providing the quantitative evaluation of the simulation of the hot-jet interference by use of a cold jet, comparisons will be made of (1) the jet boundary shape, (2) the location of shock waves produced in the external flow field surrounding each jet, (3) the static-pressure distributions in the external flow fields, and (4) the normal-force and pitching-moment coefficients corresponding to these pressure distributions.

Qualitative Consideration of Jet Interference at Transonic Speeds

In order to understand the problem of simulating jet interference of a hot jet by a cold jet, the jet patterns which control the jet interference must be understood. It was found, for both the hot and cold jets alike, that three different jet patterns occurred in the transonic speed range. These patterns are shown schematically in figure 5 and are classified as (1) subsonic, (2) near sonic, and (3) supersonic. Figure 6 presents typical schlieren photographs of the flow patterns for the three jets for the three distinct Mach number ranges. In discussing the flow patterns, it is desirable to concentrate first on the schematic flow patterns.

The subsonic pattern was characterized by a jet having an external shape that was similar to a corrugated cylinder. This type of jet is commonly referred to as a quasi-periodic jet. Another characteristic of the subsonic pattern was the mixing process that occurred on the jet boundary. The mixing was negligible in the first jet wavelength, but was increasingly significant for subsequent wavelengths. The subsonic pattern existed until M_∞ approached 1 when the near sonic pattern appeared.

The near-sonic pattern was characterized by a quasi-periodic jet shape, a mixing process on the jet boundary similar to the subsonic case, and the presence of normal shock waves which formed on the jet boundary. At low jet pressure ratios, the normal shocks were formed near the middle of each periodic length of the jet. With increasing jet pressure ratio, the shocks moved downstream toward the end of each periodic length and extended farther out into the stream. The normal shock locations were quite sensitive to free-stream Mach number. For increasing Mach number, the normal shocks moved downstream toward the end of each periodic length and at a Mach number of approximately 1.04, the near-sonic pattern changed into the supersonic pattern.

A368

The supersonic pattern was characterized by a jet having two nodes, a more rapid mixing process than for the subsonic and near-sonic cases, and an oblique shock wave emitted at the node of each of the two periods. The first shock originated near the lip of the nozzle and is usually referred to as the exit shock. It was formed from the coalescense of a series of compression waves which originated in the region near the nozzle exit. The shocks of subsequent nodal points are called jet shocks since each was a continuation of a shock from inside the jet. Two jet shocks were seen at the low jet pressure ratios, but only one was present at the higher jet pressure ratios. The disappearance of the second jet shock at the higher jet pressure ratios was due to a change in the internal jet shock structure resulting in subsonic flow immediately downstream of the first periodic jet shape.

Now that the general features of jet flow patterns at transonic speeds have been described, the schlieren photographs (fig. 6) will be examined as to details of the flow patterns. The implications, in terms of simulation of hot-jet interference, or the differences between the hot jet and either of the cold jets will be discussed subsequently. Considering first the question of jet boundary shape, it will be noted that the three jets had similar shapes only for the primary wavelength region. Each jet in this region had a distinct inviscid boundary. Farther downstream, where the previously mentioned mixing occurred along the jet boundaries, the shape of the hot-jet boundary differed considerably from that of either cold jet; the hot jet spread out more rapidly with increasing distance downstream than did the cold jets (see fig. 6(b)). The most prominent features of the portions of the flow patterns external to the jets are the previously described shock waves. From the $M_\infty = 1.0$ patterns (fig. 6(b)), it can be seen that the shock waves surrounding the hot jet were considerably different in shape from the corresponding waves for the cold jets. The hot jet produced an oblique shock on each period of the jet, whereas the cold jets produced compression fans coalescing into a normal shock. The occurrence of oblique shocks instead of normal shocks for the hot jet is quite perplexing. It could be caused by (1) the interaction of the normal shock with the sound waves emitted from the hot jet, (2) a local supersonic region due to the large wake of the hot jet, or (3) a combination of these two factors. Evidence of the sound waves being emitted from the hot and cold jets can be seen in the schlieren photographs of figure 6(a) at $M_\infty = 0.9$. Although the flow was noisy, it was steady. The sound level of the hot jet was substantially higher than that of the cold jets. At $M_\infty = 1.10$, there appears to be good agreement among the three jets as to the shape and general location of the exit shock and jet shock. Nothing can be said as to jet shocks from subsequent lengths because of insufficient definition in the schlieren photographs.

What are the implications of the foregoing qualitative comparisons of the flow patterns of the three jets in terms of simulating the external flow field interference of a hot jet by means of a cold jet? The similarity of the shapes of the jet boundaries within the primary wavelength of the three jets and the inviscid nature of these boundaries indicates the possibility of simulation of that part of the interference occurring within the primary wavelength. This indication is strengthened by the agreement as to the shape and general location of the exit and jet shocks produced by the three jets at $M_\infty = 1.10$, but is weakened by the results of the comparisons of the shocks at $M_\infty = 1.0$. Downstream of the primary wavelength, the lack of similarity noted for the boundary shapes between the hot and cold jets would seem to rule out the simulation of the interferences of these portions of the jet.

A
3
6
8

Quantitative Evaluation of the Simulation of the Interference of a Hot Jet by a Cold Jet

Jet boundary shape.- As mentioned previously, one of the variables to be compared in a quantitative evaluation of the simulation of a hot jet by a cold jet is the jet boundary shape. Measurements of jet boundary shape were limited to the primary wavelength portion of the jet. The measurements were obtained from schlieren photographs of which those of figure 6 are typical. The particular quantities measured were (1) jet primary wavelength, (2) jet diameter at the end of the primary wavelength, and (3) initial inclination of the jet boundary. These quantities are plotted in figures 7, 8, and 9, respectively. Also shown in the figures are some theoretical curves which are discussed in appendix A. The values of the primary wavelength for the three jets agreed within the experimental accuracy when compared at equal values of jet pressure ratios. This is also the case for the jet diameter at the end of the primary wavelength. Such is not the case, however, for the initial jet boundary inclination; good agreement was obtained only between the hot jet and the carbon-dioxide jet ($\gamma_j = 1.29$ for both jets at the nozzle exit). It is noted that γ_j for the two jets was not only matched at the nozzle exit, but increased approximately the same amount as the flow expanded around the nozzle lip. The boundary of the air jet ($\gamma_j = 1.4$) had lower angles of inclination at comparable jet pressure ratios. It is clear, however, that the inclination of the air jet can be made to match that of the hot jet if the air jet is operated at a different pressure ratio than that of the hot jet (e.g., $(p_j/p_\infty) = 4.5$ for the cold air jet compared to $(p_j/p_\infty) = 3.6$ for the hot jet for $\delta = 20^\circ$ at $M_\infty = 1.1$). It is equally clear from figures 7 and 8 that the air jet and hot jet would not then match as to the primary wavelength and jet diameter at the end of the primary wavelength. Thus, if simulation of the entire jet boundary within the primary wavelength region is required, both jet pressure ratios and specific heat ratios must be matched. The procedure of matching the initial jet boundary inclination of a hot jet by a cold jet at a different pressure ratio was suggested in reference 3 as a means of matching the exit shock at supersonic speeds. This procedure has often been followed by various researchers; however, there is a tendency to overlook the restriction in reference 3 that the region downstream of the initial region of the jet is not simulated.

Shock waves.- The other two variables to be compared in the quantitative evaluation of the simulation of a hot-jet interference by a cold jet are the locations of the exit and jet shock. The exit shock location was defined by the shock slope and the downstream distance from the nozzle of a point on the exit shock at some arbitrary radial distance which was chosen to be $y/d_j = 7.29$; these two variables (slope and distance) are presented in figures 10 and 11, respectively. The results for the three jets agree within the experiment accuracy. The jet shock location was specified by (1) inclination of jet shock to the free stream, (2) jet primary wavelength (i.e., location of origin of jet shock with respect to nozzle), and (3) jet diameter at the end of the primary wavelength (i.e., location of origin of shock with respect to jet center line); these variables are presented in figures 12, 7, and 8, respectively. The values of the inclination of the jet shock for the three jets agreed within the experimental accuracy when compared at the same pressure ratios. As mentioned previously, this was also the case for the jet primary wavelength and the jet diameter at the end of the primary wavelength. Thus, the locations of the shocks produced by the hot jet were adequately simulated by either of the cold jets. The question of the degree of simulation of the shock strength will be examined in the following section which presents the results of the pressure measurements.

Pressure distribution in the external flow field.- The second method of evaluating the simulation of the hot-jet interference by a cold jet was made by comparing the pressure distributions in the external flow field surrounding the hot and cold jets. Incremental static-pressure distributions in the external flow field surrounding each of the three jets are compared in figure 13 for various combinations of jet pressure ratios, Mach numbers, and test positions. As expected, three different types of pressure distributions corresponding to the subsonic, near-sonic, and supersonic flow patterns were found. In the case of the latter two distributions, shock locations determined from the schlieren photographs are indicated on the pressure-distribution plots.

The subsonic pressure distributions for all three jets were flat and differed only slightly from jet-off values. The agreement between the hot-jet and carbon-dioxide data was excellent, whereas the air-jet values were slightly lower than those for the other two jets. This indicated that the jet-temperature effect was negligible, whereas the effect of specific heat ratio was small but noticeable.

The near-sonic pressure distributions exhibited an expansion and recompression in the region of the normal shock wave. The hot-jet and carbon-dioxide data were in good agreement, whereas the air-jet data differed as much as $\Delta C_p = 0.02$ from those for the other two jets, indicating the effect of specific heat ratio.

The supersonic pressure distributions exhibited compression regions at the exit and jet shock waves. In general, the hot-jet and carbon-dioxide data agreed within the experimental accuracy for both exit and jet shock-induced compression regions at all three test positions. The differences in ΔC_p between the data for air and carbon dioxide were also small except in the region of the exit shock near the nozzle, that is, for test position I. In this region of the flow field, differences in ΔC_p of 0.03 were seen which indicated a significant effect due to specific heat ratio.

In order to see the gross effects of the simulation of a hot jet by a cold jet, the above pressure distributions were integrated to obtain incremental normal force and moment coefficients. As seen in figures 14 and 15, the effects of jet temperature on both ΔC_N and ΔC_m were small as evidenced by the small differences between the data for the hot jet and carbon dioxide. On the other hand, the effects of specific heat ratio were large. Differences in ΔC_N of 0.03 and ΔC_m of 0.015 were common between the data for air and carbon dioxide.

On the basis of the foregoing comparisons of pressure distributions and incremental normal and moment coefficients, it is concluded that the external flow field disturbances created by the hot jet at various pressure ratios were closely simulated by use of the cold-gas jet (carbon-dioxide jet) having a specific heat ratio equal to that of the hot jet. It is to be noted that this conclusion applies only to the disturbances from the primary wavelength region of the jet. As previously mentioned, jet temperature would probably be an important factor in the disturbances from subsequent portions of the jet because of the strong mixing between these portions of the jet and the surrounding flow.

The question arises as to the applicability of the foregoing conclusion to hot jets different from that tested, for example, those of higher jet pressure ratios, jet temperatures, or afterbody geometry. From the results presented herein, one is encouraged to believe that the conclusion would be applicable to those hot jets for which the flow along the primary wavelength region is essentially inviscid (i.e., mixing is negligible between the jet and the surrounding flow). Further tests will be necessary, however, to check this belief.

CONCLUSIONS

An investigation has been made of the jet boundaries and the external flow field of hot and cold sonic jets discharging into a stream whose speed was varied over the transonic range. The conclusions of the investigation are as follows:

1. The external flow was disturbed by the jets at all stream speeds. The interference was small for subsonic stream speeds and large for sonic and supersonic speeds. For the latter two speeds, the interference was the result of strong shock waves induced by the jets.

A 3 6 8

2. The interference of the hot jet was simulated satisfactorily by the cold jet when the jet pressure ratios and specific heat ratios at the exit were matched.

Ames Research Center
National Aeronautics and Space Administration
Moffett Field, Calif., Feb. 9, 1961

APPENDIX A

JET PROPERTIES

In the course of the investigation, some interesting jet properties were studied, namely, the effects of jet pressure ratio and free-stream Mach number on the jet periodicity, internal jet structure, primary wavelength, jet boundary, and shock waves. These jet properties together with some theoretical results are presented in this appendix.

QUASI-PERIODIC NATURE OF JET

Over part of the jet pressure ratio and stream Mach number ranges, the jets exhibited a quasi-periodic nature which is characteristic of sonic and supersonic jets discharging into quiescent air or a subsonic stream. This phenomenon was known to exist as early as the experiments of Rayleigh in 1879. Many explanations based on the compression and expansion wave mechanism within the jet have been offered; a summary is given in reference 8. Typical schlieren photographs showing the quasi-periodic nature are given in figure 6. Note that the periodicity existed only at the lower jet pressure ratios. Another factor which affected the periodicity was the stream Mach number. It was found that the periodicity existed only at the subsonic and sonic stream Mach numbers. This confirmed the theoretical results of reference 8 which stated that the periodicity existed only at subsonic Mach numbers.

INTERNAL JET STRUCTURE

The internal jet structure was found to be of two types. The first type occurred at low jet pressure ratios and consisted of an intersecting oblique shock pattern commonly called shock diamonds (see fig. 6). A detailed drawing showing the formation of the oblique shocks as constructed by the method of characteristics is illustrated in reference 12. The second type of internal jet structure appeared as the jet pressure ratio increased above 2. The jet structure then had a series of circular, dish-shaped normal shocks, often referred to as Riemann waves. Reference 3 showed that the second type also existed at higher jet pressure ratios than those of the present investigation.

PRIMARY WAVELENGTH

Since the observations of Rayleigh, many theories have been advanced for the prediction of the primary wavelength. Among these, the following theories were chosen for comparison: (1) semiempirical theory of reference 11 for a sonic jet in still air, (2) linear theory of reference 16 for a sonic jet in a stream of any Mach number, and (3) first-order theory of reference 10 which was modified (see appendix B) so that it was applicable to a sonic jet in a supersonic stream. Where the present data were compared with the theories (fig. 7), the semiempirical theory (ref. 11) was found to agree with the data quite well. The agreement was rather surprising since the theory was for a jet in still air whereas the present data was for a jet in a supersonic stream. The linear theory (ref. 16) approximated the data well only for jet pressure ratio up to 2. Of course, this was expected since linear theory assumed the jet pressure ratio to be small. The agreement between the modified first-order theory (ref. 10 and appendix B) and the experimental data was poor at low and high jet pressure ratios. The modified first-order theory also showed that w/d_j was dependent on γ_j which was contrary to the experimental data.

The effect of jet pressure ratio on w was large, whereas the effect of stream Mach number was small. In fact, the transonic data agree quite well with the data of reference 3 for $M_\infty = 0$.

DIAMETER AT END OF PRIMARY WAVELENGTH

The experimental values of the jet diameter at the end of the primary wavelength are compared with theoretical values obtained by modification of the theory of reference 10 (see eq. (B13)). The theory predicts a diameter equal to the nozzle diameter (see fig. 8), a result which is in agreement with experiment to a pressure ratio of 4.

INITIAL INCLINATION OF JET BOUNDARY

It is known that an underexpanded jet will undergo a two-dimensional expansion at the nozzle lip. The degree of expansion depends on the jet pressure ratio and the specific heat ratio. The effects of these variables on the expansion angle, or the initial inclination of jet boundary, δ, are shown in figure 9. The effect of jet pressure ratio was large. The value of δ varied from 5° to 28° for jet pressure ratios from 2 to 6. As mentioned previously, the effect of specific heat ratio was large as evidenced by the differences between the air and carbon-dioxide data. The value of δ was not affected appreciably by the jet temperature or stream Mach number. Theoretical results, based on a two-dimensional expansion wave at the nozzle (see ref. 9), were in good agreement with experimental data. The effects of specific heat ratio were also predicted quite well by the theory.

JET SHOCK INCLINATION ANGLE

The jet shock inclination angle α was discussed previously in respect to jet temperature and specific heat ratio. However, since the α data at higher stream Mach numbers were readily available in references 5, 6, and 7, the effect of M_∞ on α is presented in figure 12. It was found that α varied from 31.5° at $M_\infty = 2.02$ to approximately 60° to 65° at $M_\infty = 1.1$. (Although not shown in the figure, it was found that α approached 90°, normal shock, at M_∞ near 1.04.) Also shown are the Mach angles for the corresponding M_∞. The agreement of α with the Mach angle was within 3 percent at M_∞ greater than 1.39 and within 10 percent at $M_\infty = 1.1$. This indicated that α could be estimated to at least 10-percent accuracy by its Mach angle.

APPENDIX B

CALCULATION OF THE PRIMARY WAVELENGTH AND THE JET DIAMETER AT THE END OF THE PRIMARY WAVELENGTH

Reference 10 gave a method for calculating the initial contour of a supersonic jet in a supersonic stream. For the case of a sonic jet, the method of reference 10 was not directly applicable. Hence a modification was made and is shown below.

The potential flow equation for an axisymmetric supersonic jet is

$$\varphi_{yy} + \frac{1}{y}\varphi_y - B_j^2\varphi_{xx} = 0 \tag{B1}$$

where φ_x and φ_y denote partial derivatives with respect to x and y, respectively.

The equation for a sonic jet is

$$\varphi_{yy} + \frac{1}{y}\varphi_y - A_j^2\varphi_{xx} = 0 \tag{B2}$$

where

$$A_j^2 = \frac{\gamma+1}{V_\infty}\varphi_x$$

If φ_x is assumed to be a positive constant, then equations (B1) and (B2) are equivalent with $A_j^2 = B_j^2$. From the first order theory of reference 10, the equation for the jet radius variation from the nozzle radius is

$$\frac{d^2R}{dx^2} + b_1\frac{dR}{dx} + b_2R = 0 \tag{B3}$$

The first order solution is then

$$R = \frac{\delta \sin\sqrt{b_2 - (b_1^2/4)}\; x}{\sqrt{b_2 - (b_1^2/4)}\; e^{b_1 x/4}} \tag{B4}$$

for

$$0 < x/A_j d_j < 4 \tag{B5a}$$

and

$$b_2 > b_1^2/4 \tag{B5b}$$

The limitations of (B5a) and (B5b) will be discussed later.

The constants b_1 and b_2 are

$$b_1 = -\frac{a_2}{d_j a_1} \tag{B6a}$$

$$b_2 = \frac{3}{2}\frac{a_3}{A_j d_j a_1} \tag{B6b}$$

where

$$a_1 = \frac{\rho_\infty V_\infty^{\,2}}{\rho_j V_j^{\,2}}\frac{1}{B_\infty} + \frac{1}{A_j} \tag{B6c}$$

A368

$$a_2 = \frac{\rho_\infty V_\infty^{\,2}}{\rho_j V_j^{\,2}}\frac{1}{B_\infty^{\,2}} - \frac{1}{A_j^{\,2}} \tag{B6d}$$

$$a_3 = \frac{\rho_\infty V_\infty^{\,2}}{\rho_j V_j^{\,2}}\frac{A_j}{B_\infty^{\,3}} + \frac{1}{A_j^{\,2}} \tag{B6e}$$

The constants b_1 and b_2 can be found if A_j and a_1 are known. The constant a_1 can be found from the first-order theory of reference 10 which gives

$$\delta = \frac{1 - (p_\infty/p_j)}{a_1\gamma_j} \quad \text{or} \quad a_1 = \frac{1 - (p_\infty/p_j)}{\delta\gamma_j} \tag{B7}$$

In general, δ is not known a priori. In order to find δ, the method of reference 9 can be used. It gives an expression of the type

$$\delta = C(\gamma_j)(p_j/p_\infty) \tag{B8}$$

where $C(\gamma_j)$ is approximately 6 to 6.5 for $\gamma = 1.4$ to 1.28. From equations (B6c), (B7), (B8), it follows that

$$A_j = \frac{p_j/p_\infty}{6 - (p_j/p_\infty)}$$

Now the restrictions of equation (B5a) can be seen to be

$$0 < \frac{x}{d_j}\,\frac{6 - (p_j/p_\infty)}{p_j/p_\infty} < 4 \tag{B9}$$

which means that p_j/p_∞ must be less than 6. Now to check the limitations of equation (B5b), it can be shown that

$$b_2 - \frac{b_1^2}{4} = \frac{2}{d_j}\left[\frac{C_1}{(p_j/p_\infty)^2} + \frac{C_2}{p_j/p_\infty} + C_3\right]$$

where C_1, C_2, and C_3 are positive constants. Therefore, it is seen that $b_2 > b_1^2/4$ for all p_j/p_∞ and hence equation (B5b) is satisfied.

The jet primary wavelength can be found from equation (B4). It is seen that the jet periods are located at the zeros of the sine function, that is

$$\sin\sqrt{b_2 - (b_1^2/4)}\; x = 0 \tag{B10}$$

or

$$\sqrt{b_2 - (b_1^2/4)}\; x = n\pi/2, \qquad n = 1, 2, 3, \ldots \tag{B11}$$

At the primary wavelength, n = 1 and equation (B11) becomes

$$w = \frac{\pi}{2\sqrt{b_2 - (b_1^2/4)}} \tag{B12}$$

The jet diameter at the end of the primary wavelength is by definition located at $x = w$. Therefore equation (B4) becomes

$$R = 0$$

or

$$R = \frac{1}{2}(d_w - d_j) = 0$$

$$d_w = d_j \tag{B13}$$

Therefore, the jet diameter at the end of the primary wavelength is equal to the nozzle diameter.

REFERENCES

1. Peck, Robert F.: Jet Effects on Longitudinal Trim of An Airplane Configuration Measured at Mach Numbers Between 1.2 and 1.8. NACA RM L54J29a, 1955.

2. Pitts, William C., and Wiggins, Lyle E.: Axial-Force Reduction by Interference Between Jet and Neighboring Afterbody. NASA TN D-332, 1960.

3. Love, Eugene S., and Grigsby, Carl E.: Some Studies of Axisymmetric Free Jets Exhausting From Sonic and Supersonic Nozzles Into Still Air and Into Supersonic Streams. NACA RM L54L31, 1955.

4. Bressette, Walter E.: Some Experiments Relating to the Problem of Simulation of Hot Jet Engines in Studies of Jet Effects on Adjacent Surfaces at a Free-Stream Mach Number of 1.80. NACA RM L56E07, 1956.

5. Bressette, Walter E., and Leiss, Abraham: Investigation of Jet Effects on a Flat Surface Downstream of the Exit of a Simulated Turbojet Nacelle at a Free-Stream Mach Number of 1.39. NACA RM L55L13, 1956.

6. Bressette, Walter E.: Investigation of the Jet Effects on a Flat Surface Downstream of the Exit of a Simulated Turbojet Nacelle at a Free-Stream Mach Number of 2.02. NACA RM L54E05a, 1954.

7. Leiss, Abraham, and Bressette, Walter E.: Pressure Distribution Induced on a Flat Plate by a Supersonic and Sonic Jet Exhaust at a Free-Stream Mach Number of 1.80. NACA RM L56I06, 1957.

8. Pai, Shih-i: Fluid Dynamics of Jets. D. Van Nostrand Co., Inc., New York, 1954.

9. Love, Eugene S.: Initial Inclination of the Mixing Boundary Separating An Exhausting Supersonic Jet From a Supersonic Ambient Stream. NACA RM L55J14, 1956.

10. Englert, Gerald W.: Operational Method of Determining the Initial Contour of and Pressure Field About a Supersonic Jet. NASA TN D-279, 1960.

11. Hartmann, Julius, and Lazarus, Freimut: The Air-Jet With a Velocity Exceeding That of Sound. Phil. Mag. and Jour. Sci., ser. 7, vol. 31, no. 204, Jan. 1941, pp. 35-50.

12. Schäfer, M.: Steady Supersonic Flows. British M.A.P. Volkenrode. Reps. and Trans. 995, April 15, 1948; Reps. and Trans. 996, May 1, 1948.

13. Kawamura, Ryuma: Reflection of a Wave at an Interface of Supersonic Flows and Wave Patterns in a Supersonic Compound Jet. Jour. Physical Soc. of Japan, vol. 7, no. 5, Sept.-Oct. 1952, pp. 482-485.

14. Swihart, John M., and Crabill, Norman L.: Steady Loads Due to Jet Interference on Wings, Tails, and Fuselages at Transonic Speeds. NACA RM L57D24b, 1957.

15. Knechtel, Earl D.: Experimental Investigation at Transonic Speeds of Pressure Distributions Over Wedge and Circular-Arc Airfoil Sections and Evaluations of Perforated-Wall Interference. NASA TN D-15, 1959.

16. Pack D. C.: A Note on Prandtl's Formula for the Wave-Length of a Supersonic Gas Jet. Quart. Jour. Mech. and Appl. Math., vol. III, pt. 2, June 1950, pp. 173-181.

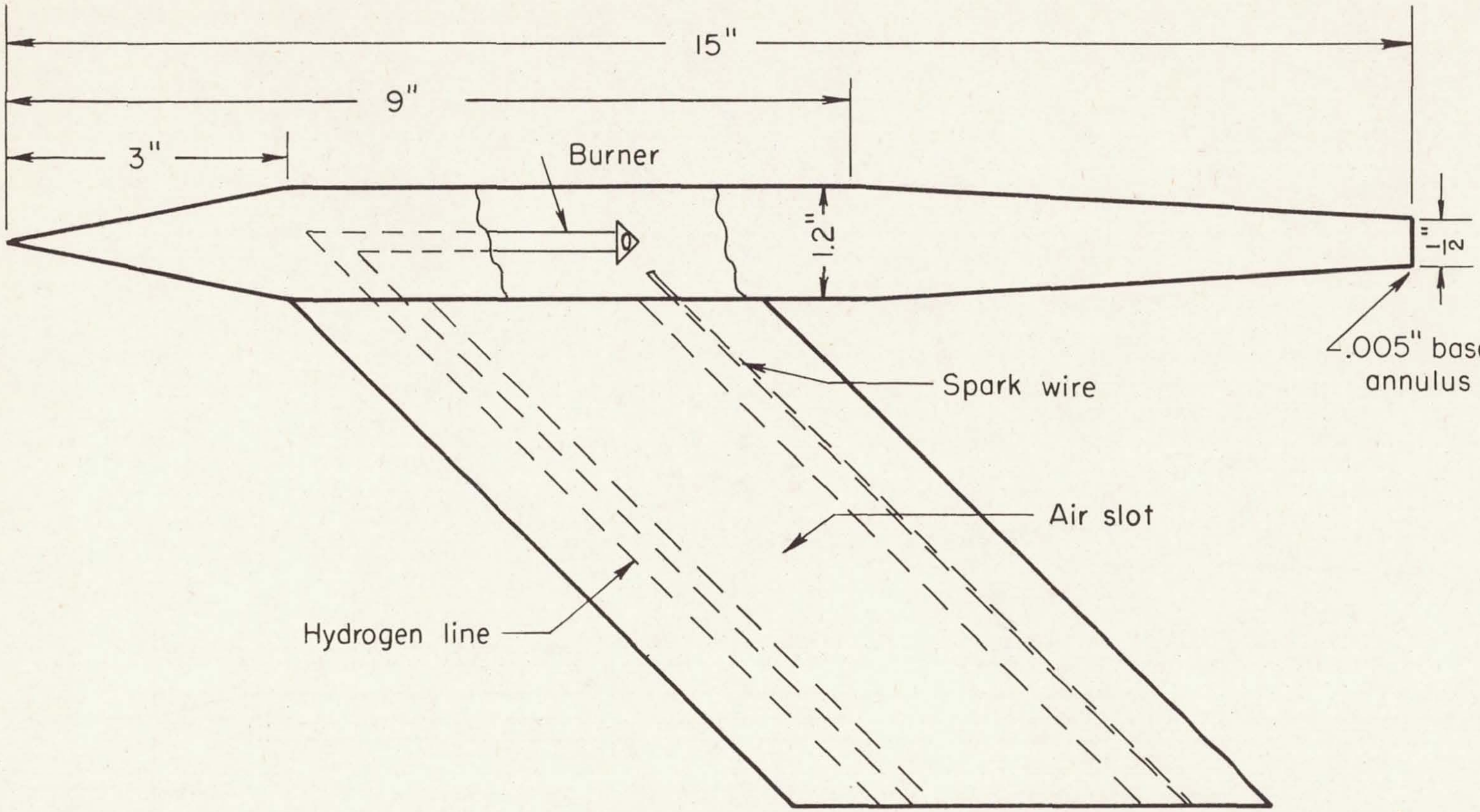

Figure 1.- Geometric details of model.

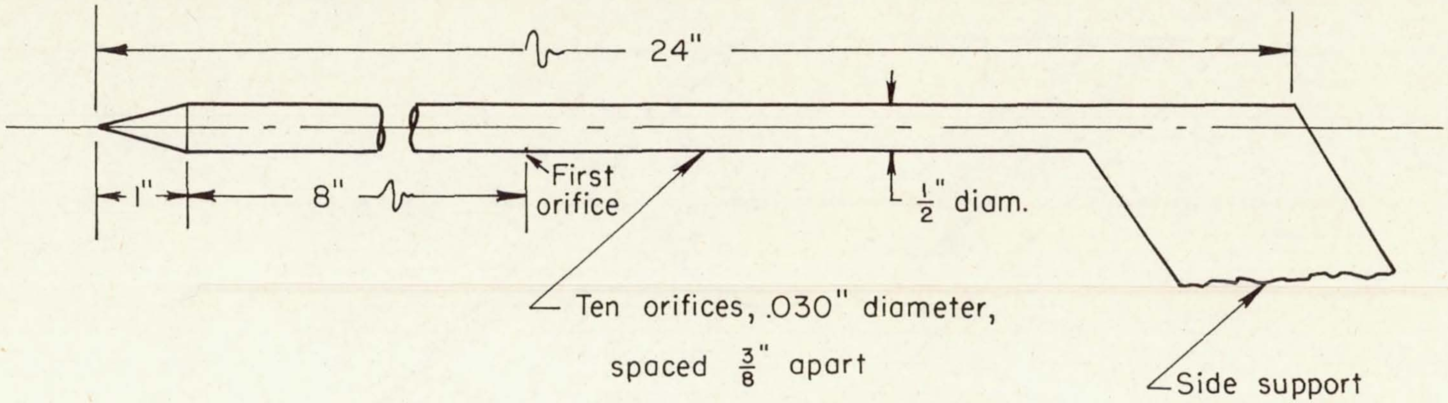

Figure 2.- Geometric details of pressure survey tube.

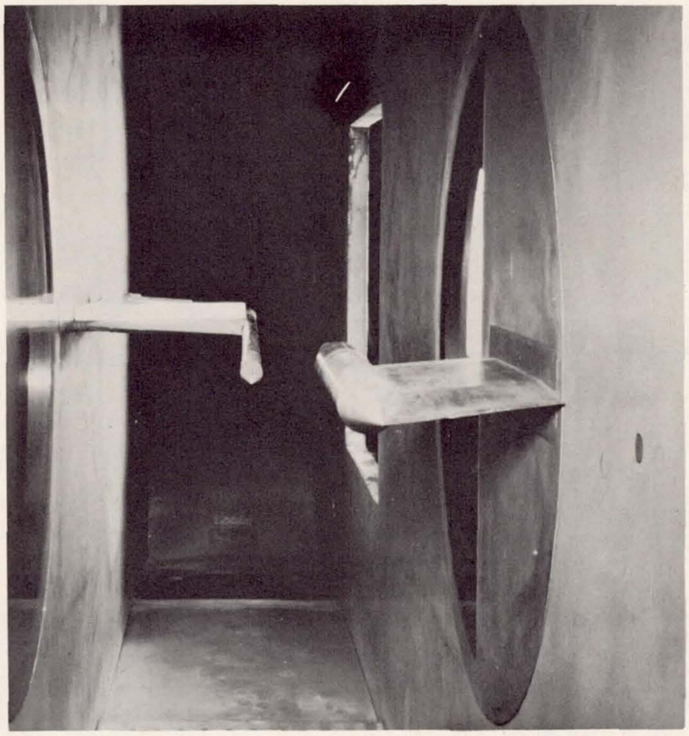

A-25638

Figure 3.- Photograph of model and pressure survey tube mounted in tunnel.

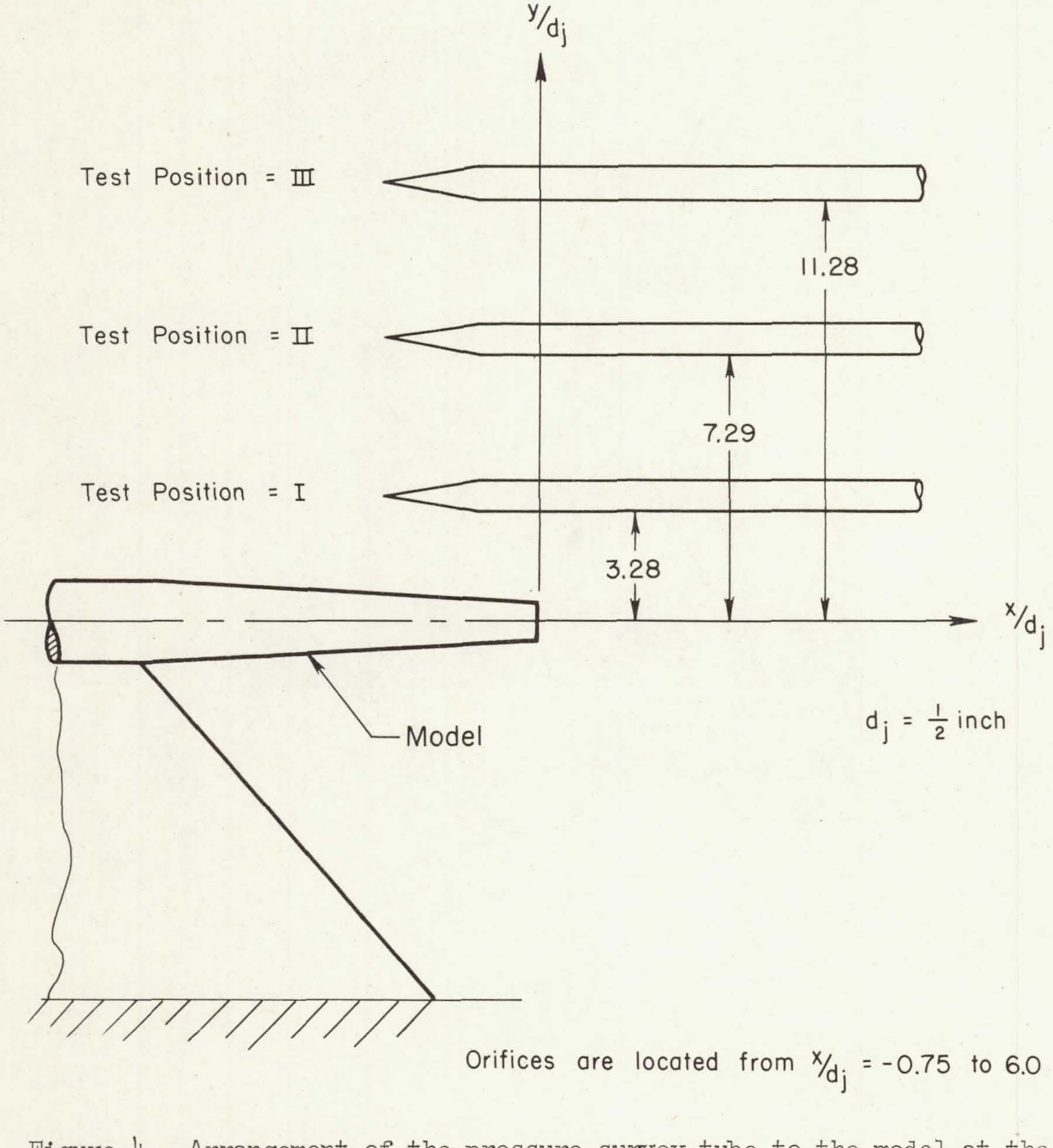

A
3
6
8

Figure 4.- Arrangement of the pressure survey tube to the model at the three test positions.

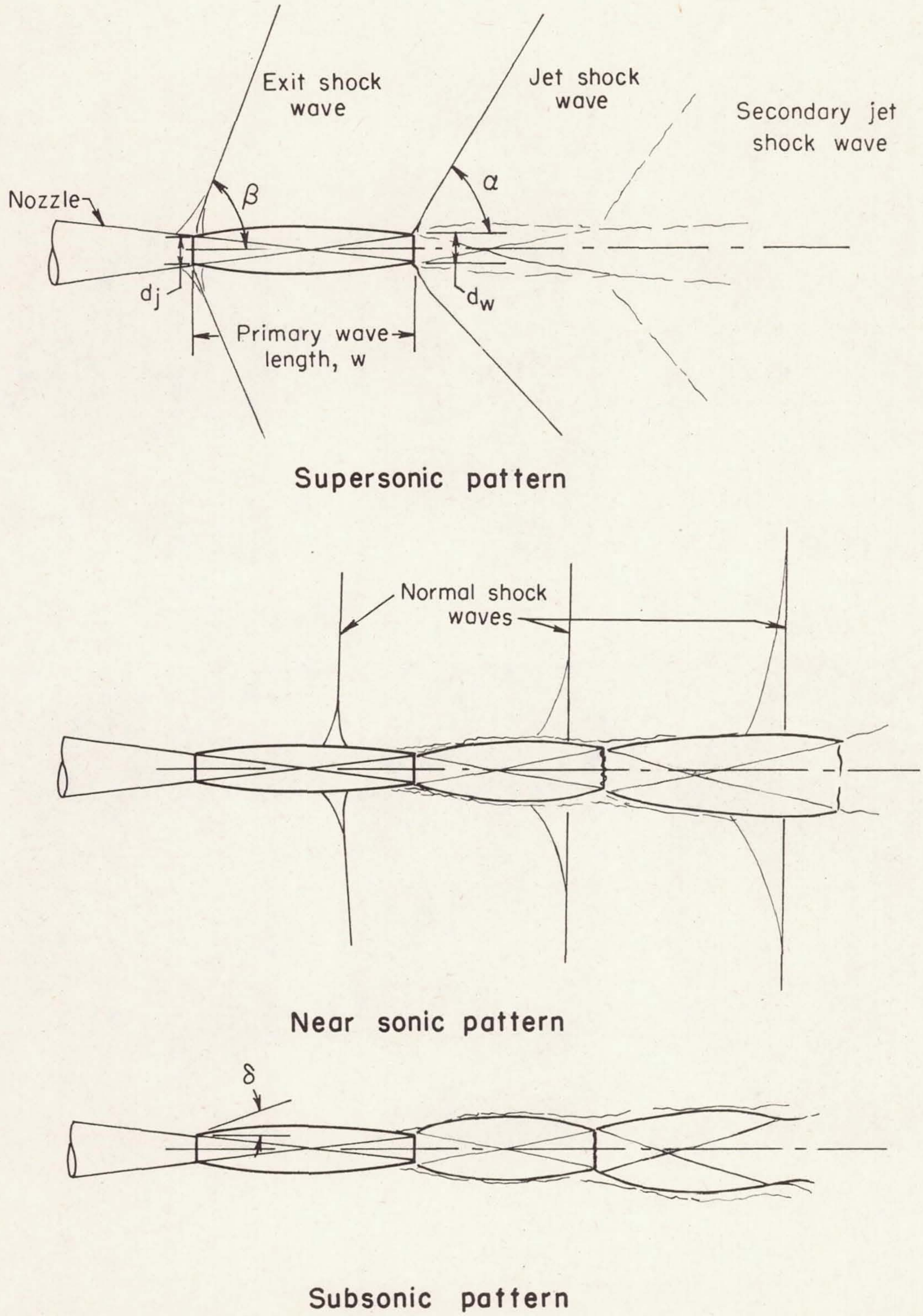

Figure 5.- Typical jet aerodynamic interference patterns.

A
3
6
8

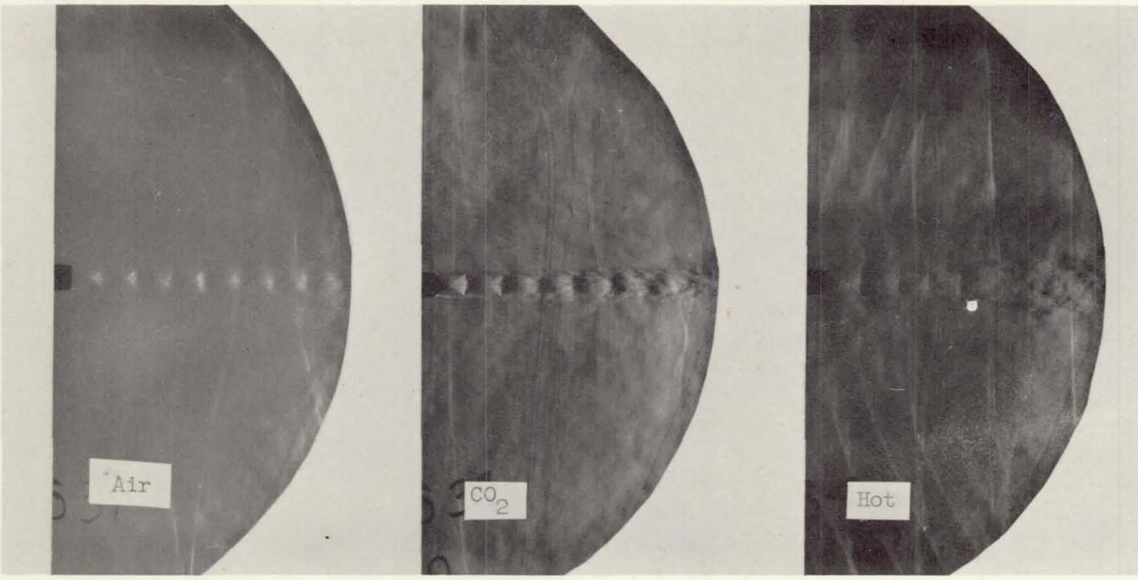

p_j/p_∞ = 1.77 p_j/p_∞ = 1.77 p_j/p_∞ = 1.76

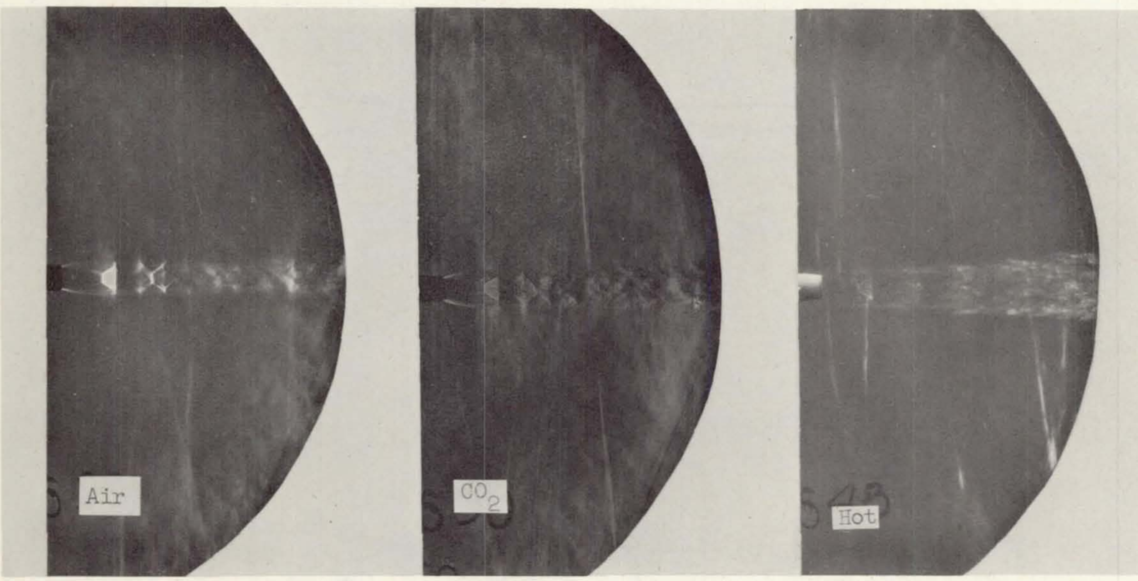

p_j/p_∞ = 3.77 p_j/p_∞ = 3.74 p_j/p_∞ = 3.82

(a) M_∞ = 0.90

Figure 6.- Schlieren photographs of the hot, carbon dioxide and air jets discharging into a transonic free stream.

A
3
6
8

A
3
6
8

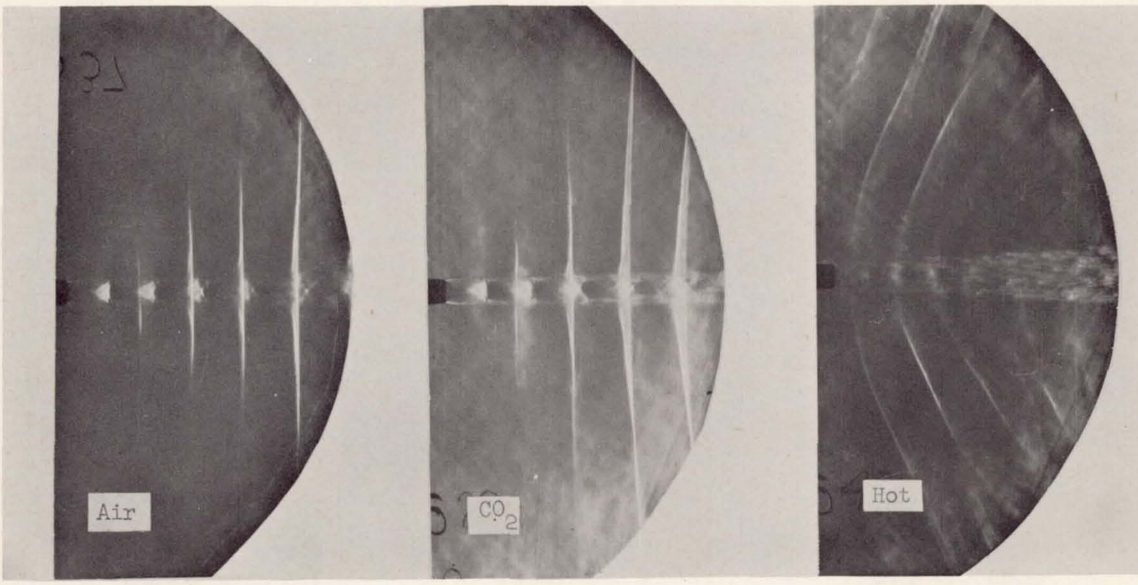

$p_j/p_\infty = 2.30$ $p_j/p_\infty = 2.24$ $p_j/p_\infty = 2.29$

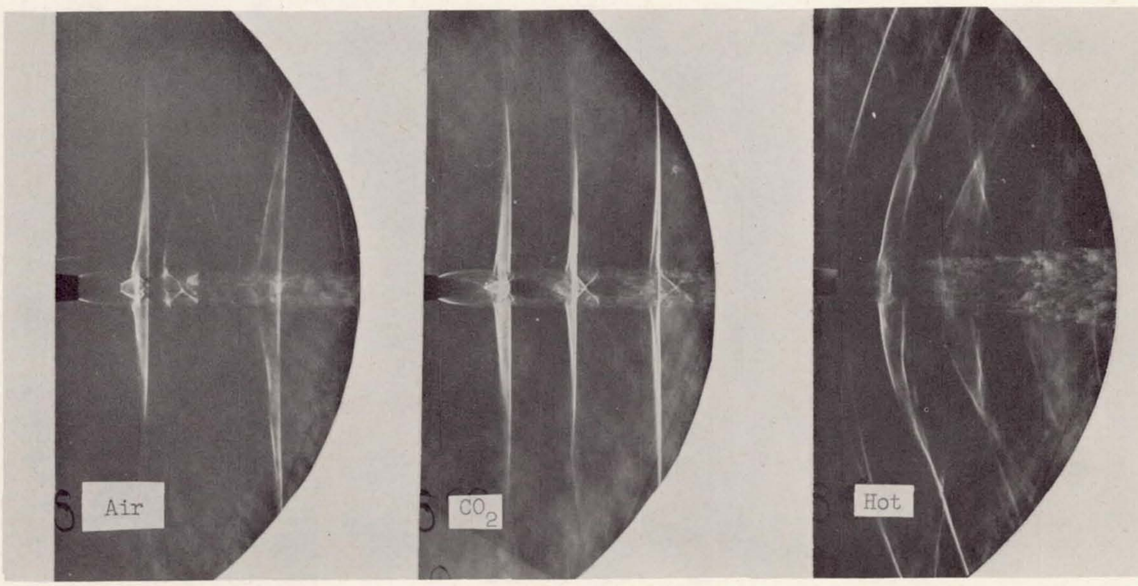

$p_j/p_\infty = 4.06$ $p_j/p_\infty = 3.96$ $p_j/p_\infty = 3.93$

(b) $M_\infty = 1.00$

Figure 6.- Continued.

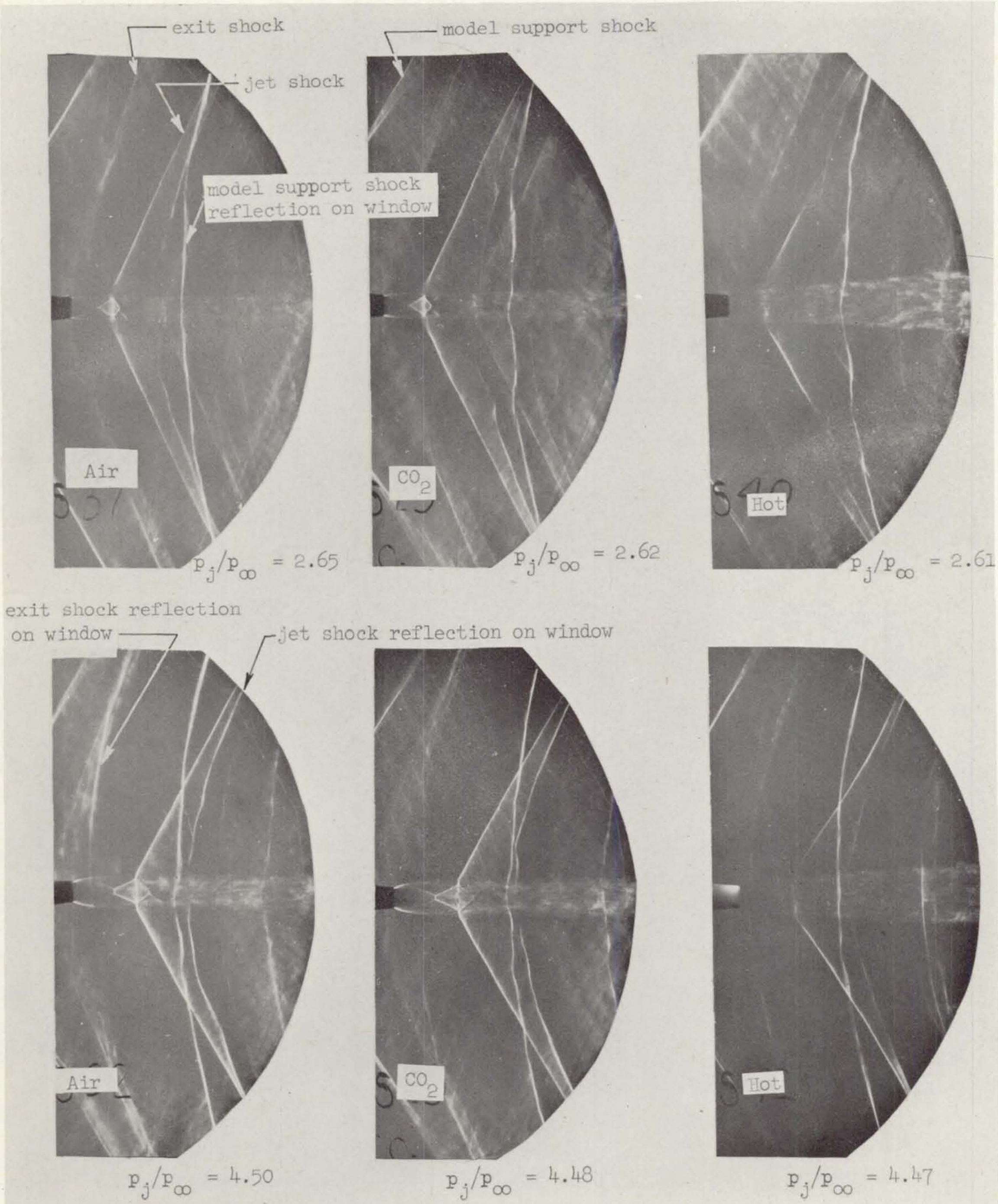

(c) $M_\infty = 1.10$

Figure 6.- Concluded.

A
3
6
8

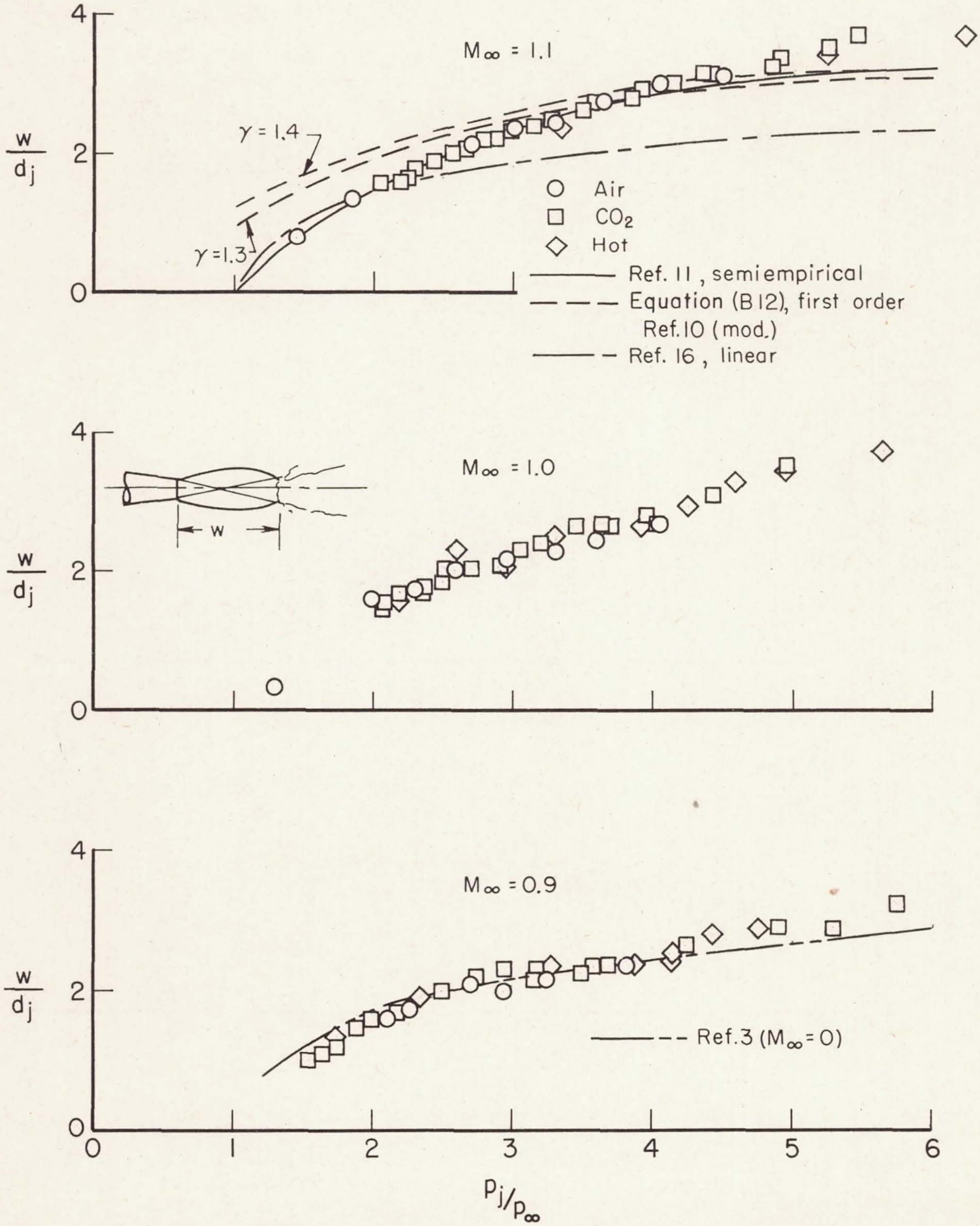

A
3
6
8

Figure 7.- Effects of jet temperature and specific heat ratio on the jet primary wavelength.

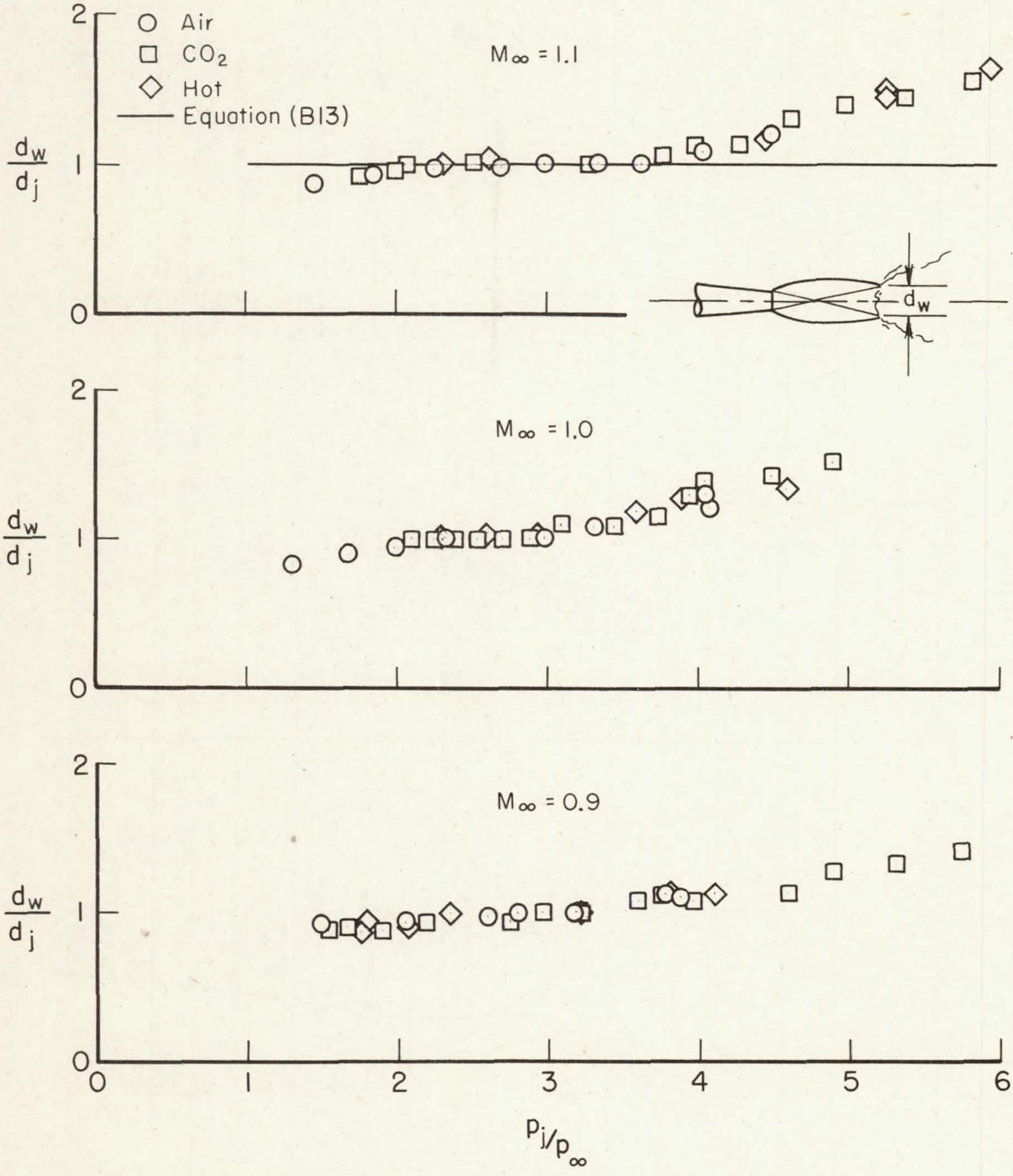

Figure 8.- Effects of jet temperature and specific heat ratio on the jet diameter at end of the primary wavelength.

A
3
6
8

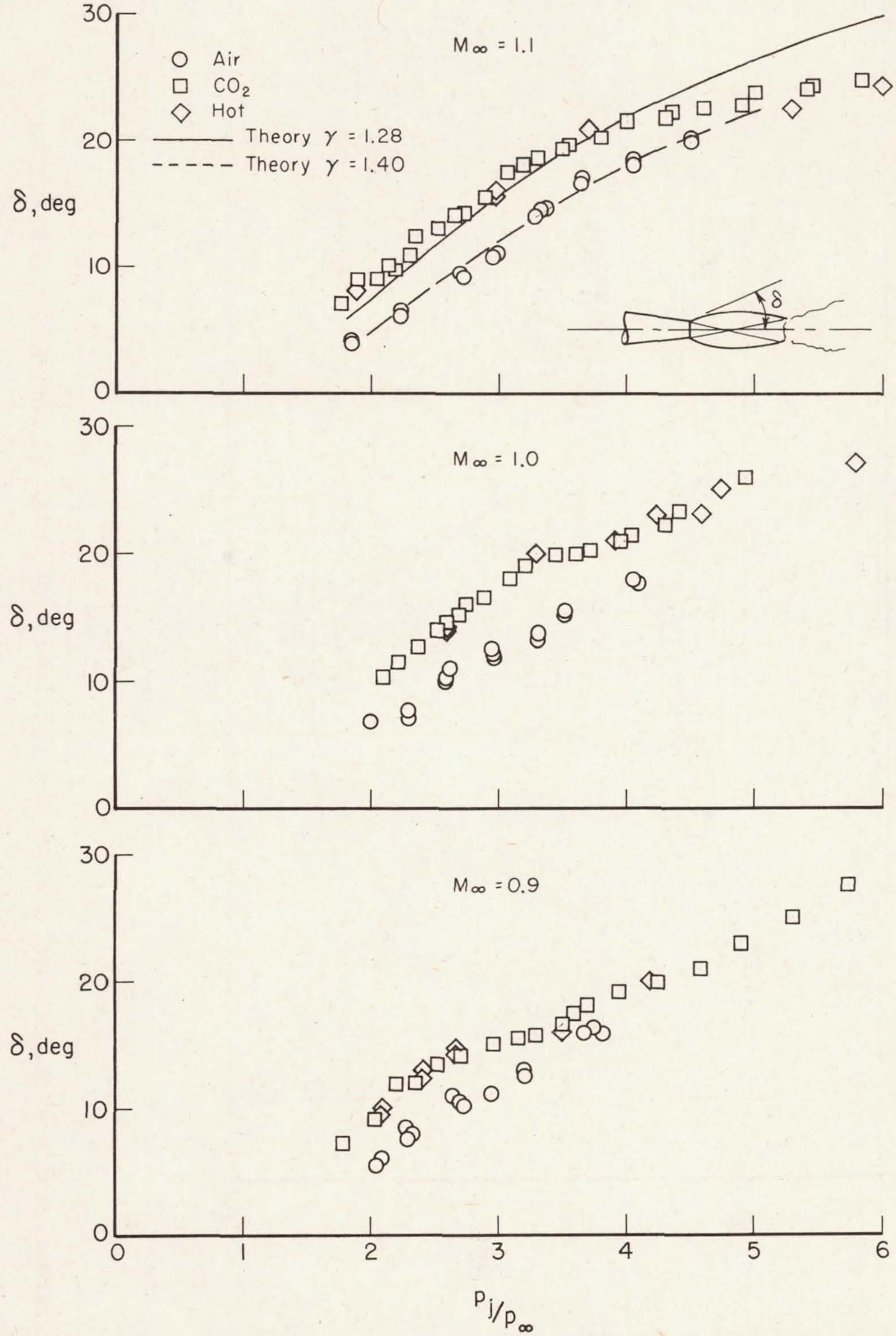

A
3
6
8

Figure 9.- Effects of jet temperature and specific heat ratio on the initial inclination of the jet boundary.

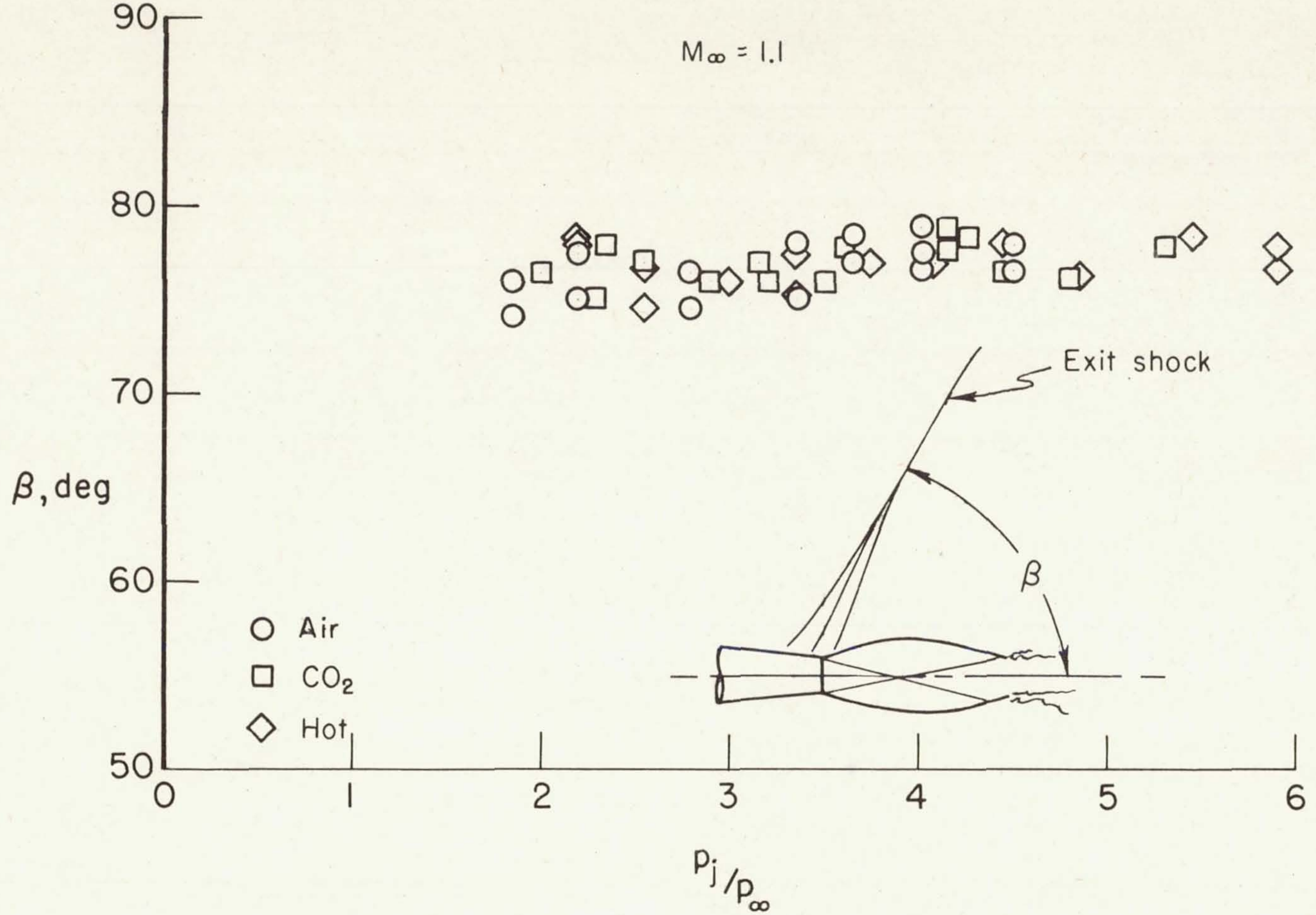

Figure 10.- Effect of jet temperature and specific heat ratio on the exit shock inclination.

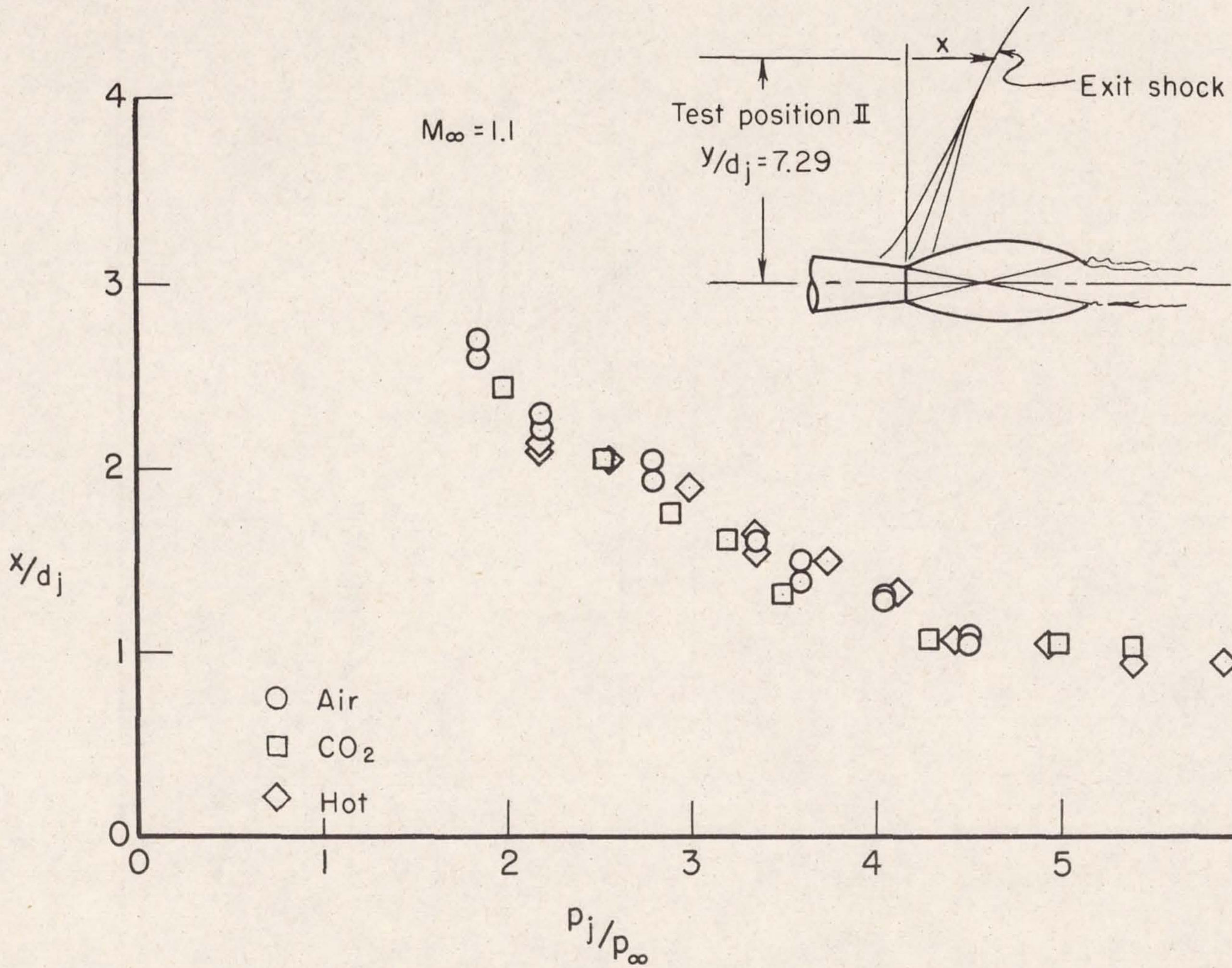

Figure 11.- Effect of jet temperature and specific heat ratio on the intersection of the exit shock at $y/d_j = 7.29$.

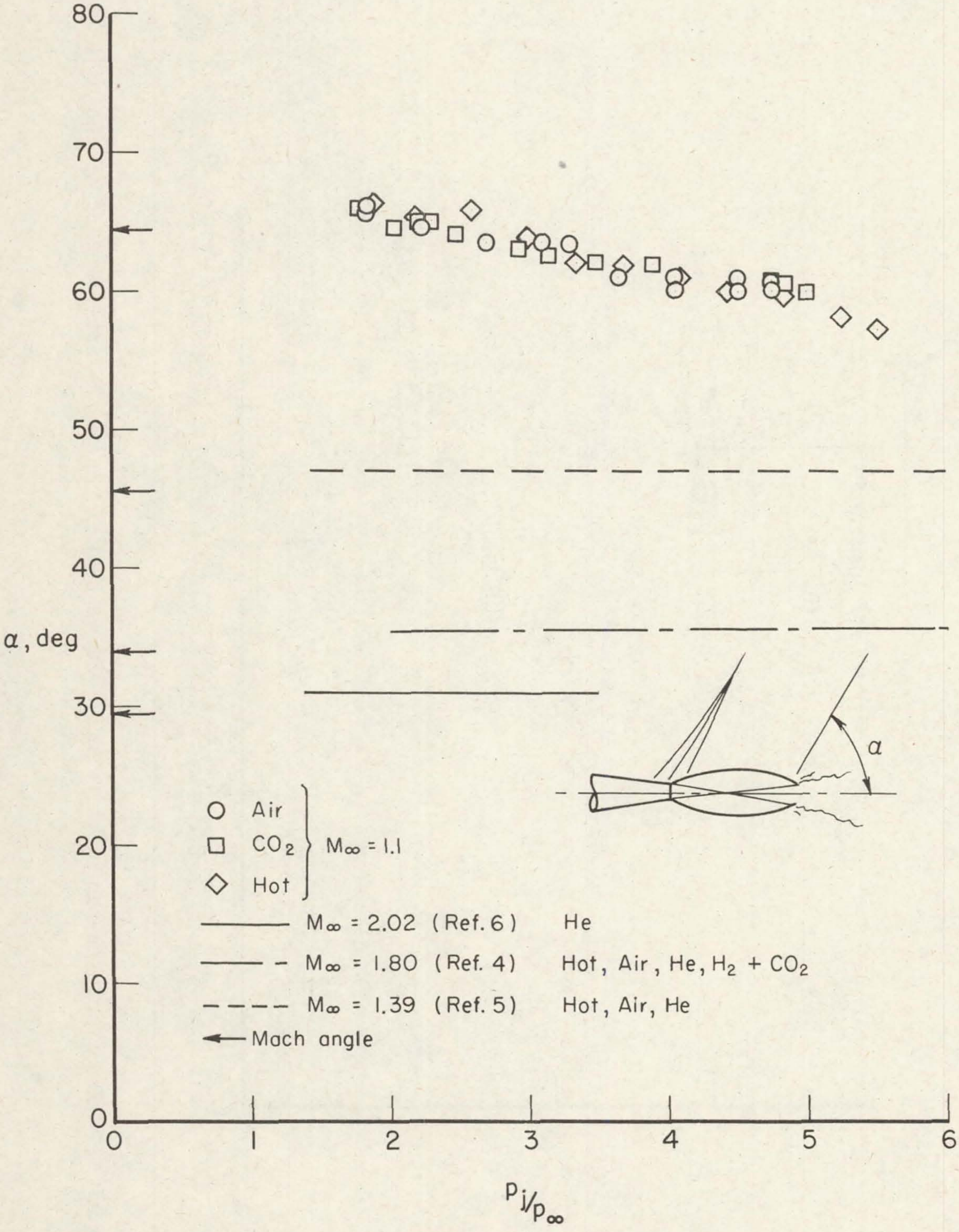

Figure 12.- Effects of jet temperature and specific heat ratio and Mach number on the jet shock inclination angle.

A
3
6
8

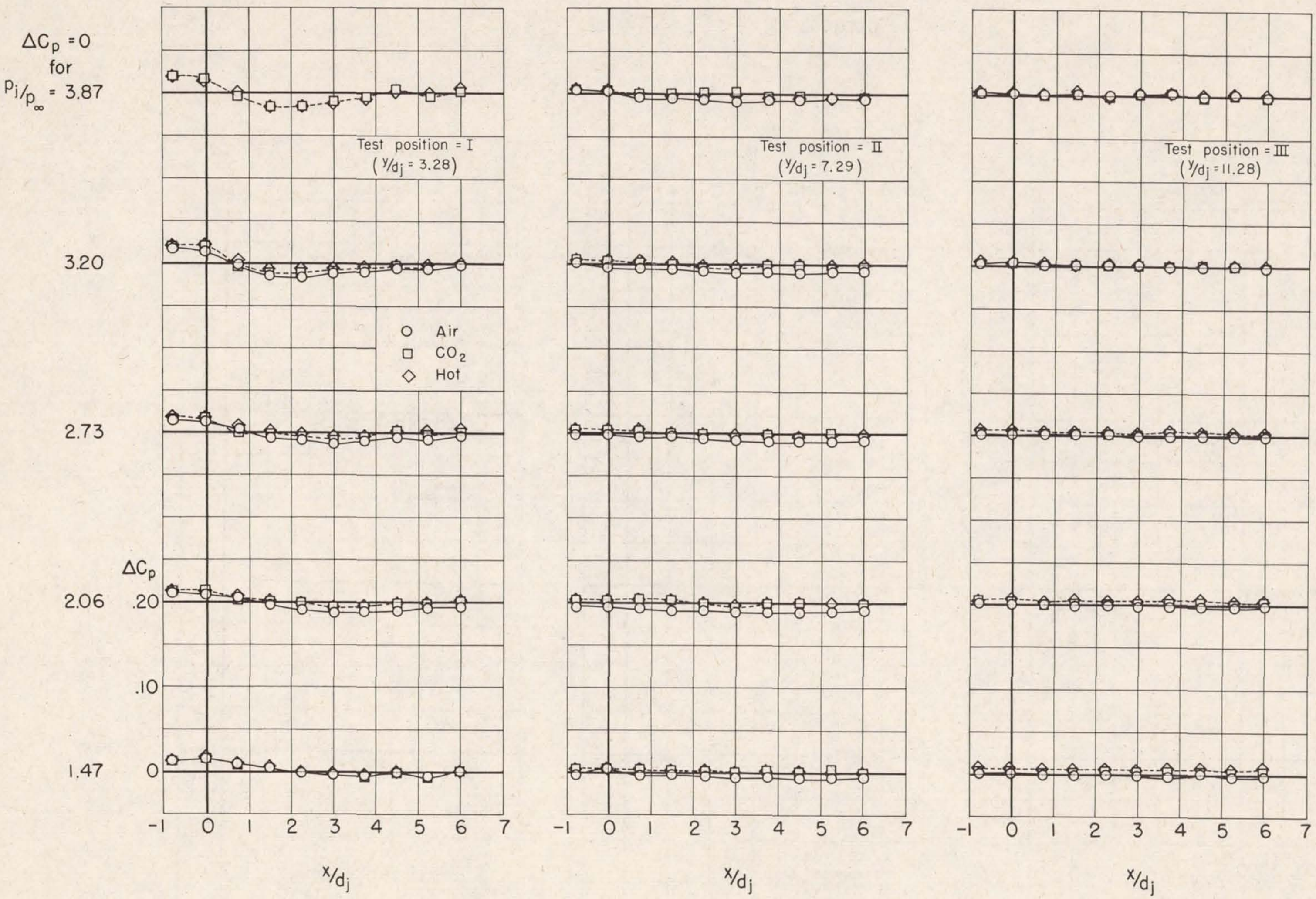

(a) $M_\infty = 0.90$

Figure 13.- Variation of incremental pressure coefficients for all three test positions.

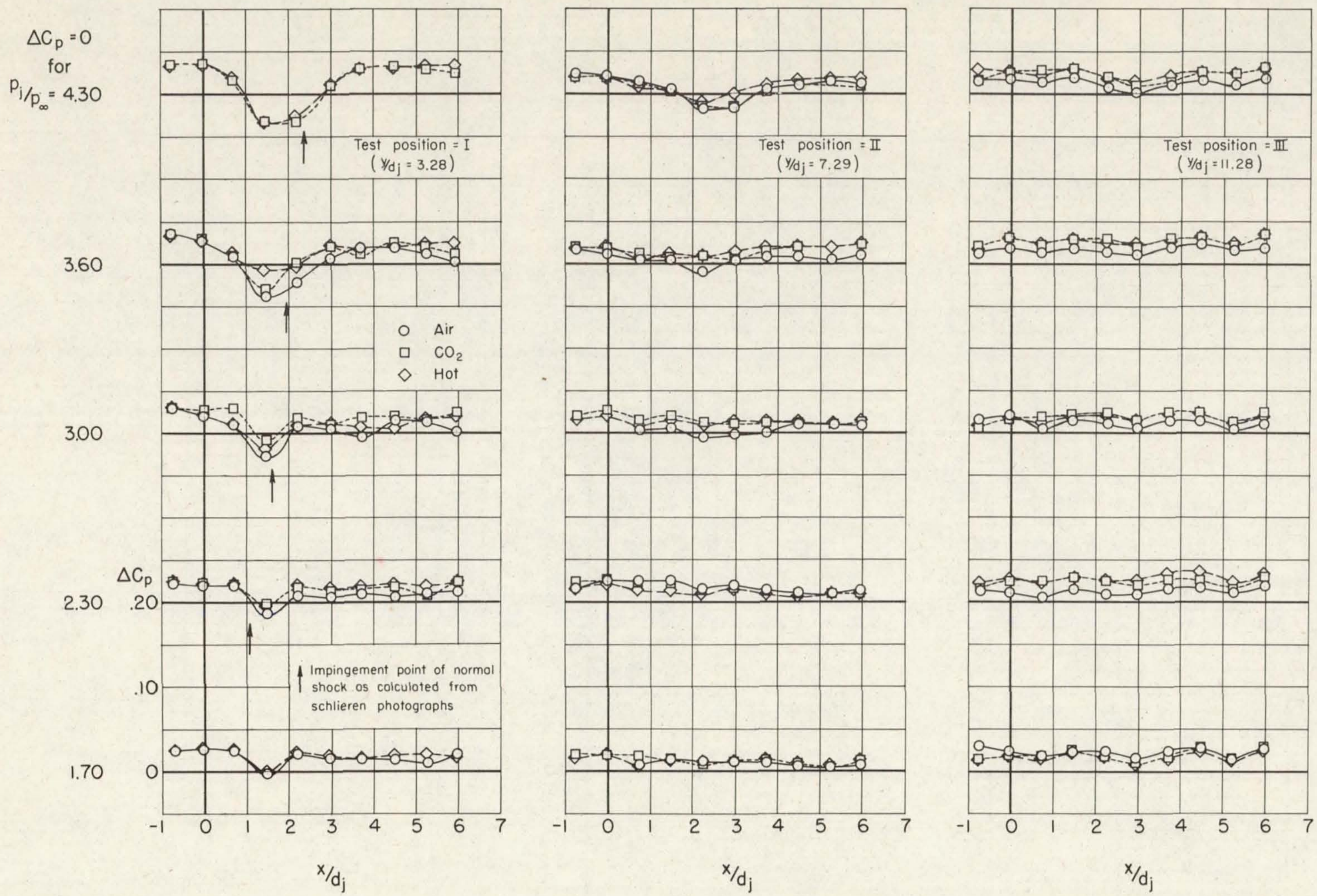

(b) $M_\infty = 1.00$

Figure 13.- Continued.

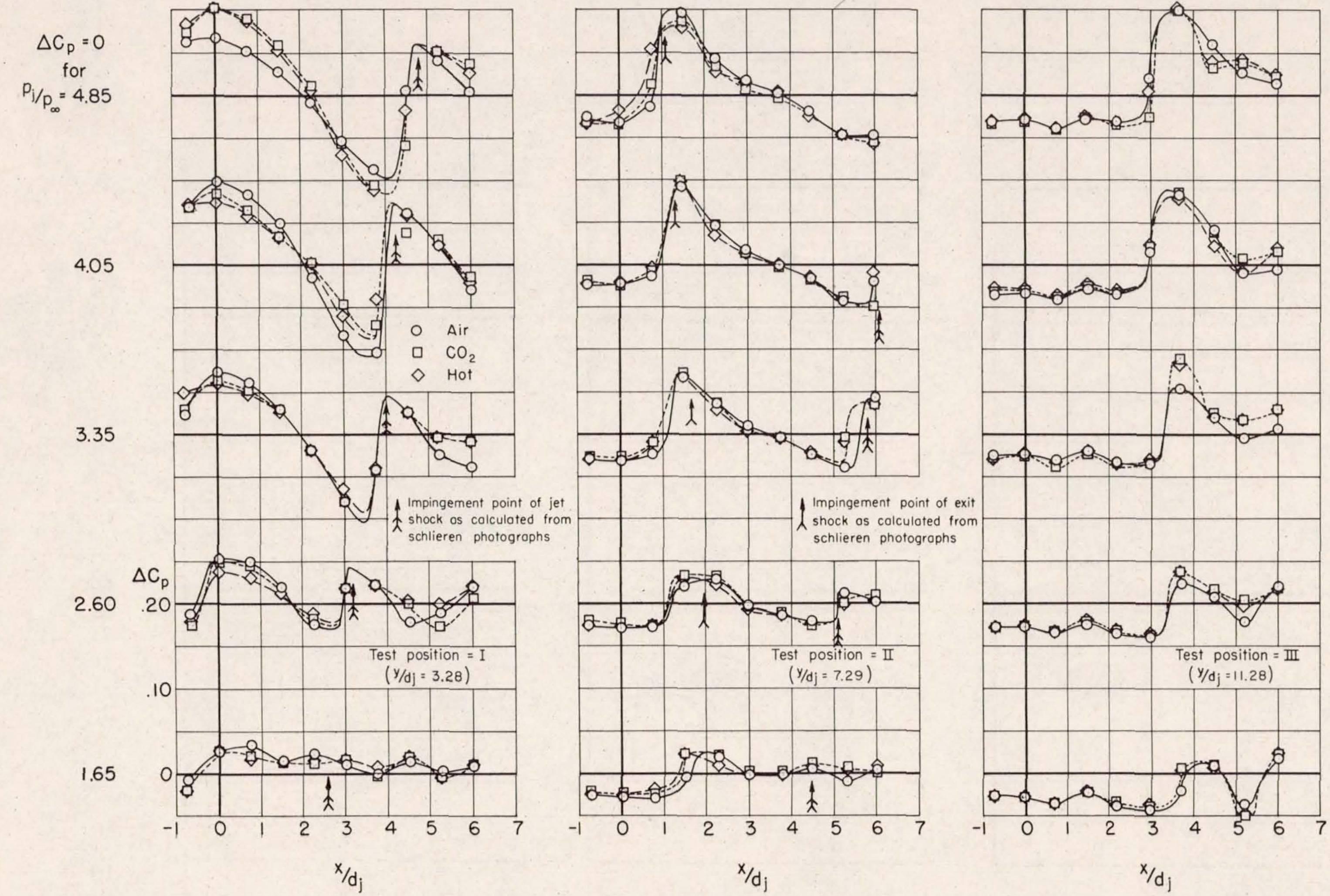

(c) $M_\infty = 1.10$

Figure 13.- Concluded.

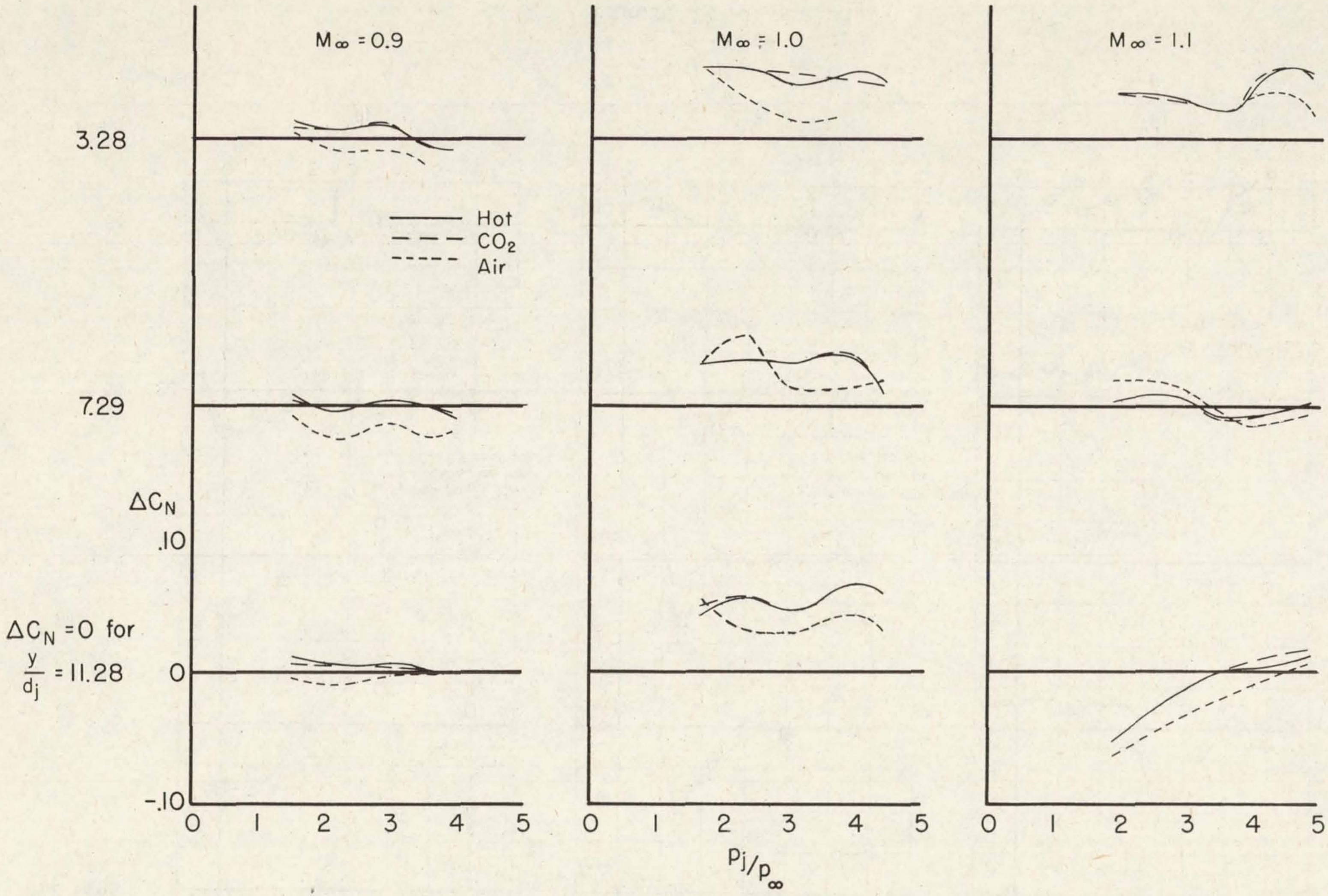

Figure 14.- Effects of jet temperature and specific heat ratio on the incremental normal force coefficient.

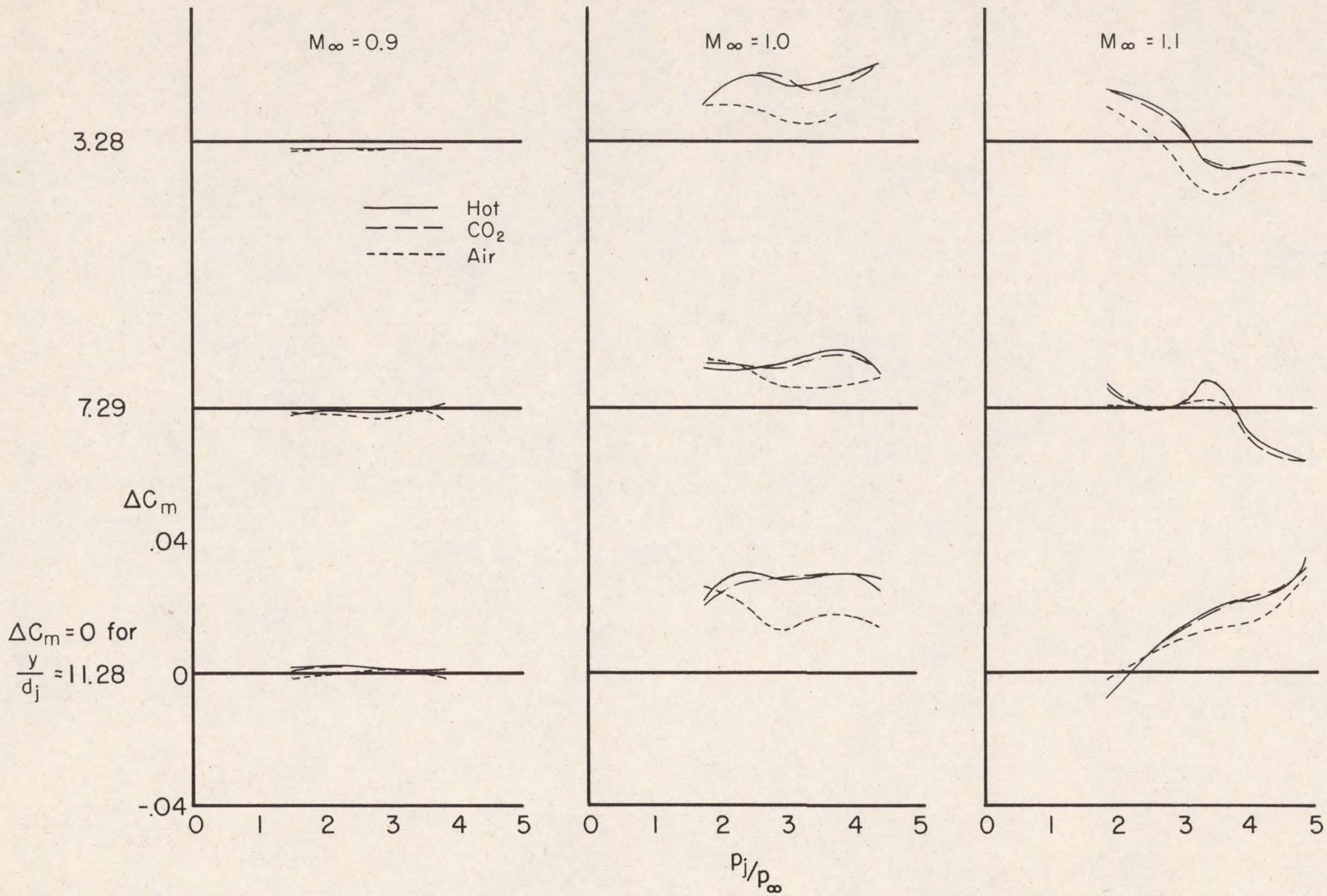

Figure 15.- Effects of jet temperature and specific heat ratio on the incremental moment coefficient.